

Characterization of Multipath Acoustic Channels in very Shallow Waters for Communications

Tan Bien Aik, Quek Swee Sen, Zou Nan

DSO National Laboratories, 20 Science Park Drive, Singapore 118230.

Email: tbienaik@dso.org.sg

Abstract – The motivations for studying the channel characteristics of a very shallow water environment are twofold: One, to account for the poor performance of commercial off the shelf (COTS) underwater acoustic modems in warm, very shallow waters and two, to design realistic channel models and communication systems which are able to perform in such an environment. This paper presents an experimental analysis of medium frequency (9-28kHz) channel measurements in very shallow waters (15-30m) for transmission distance ranging from 80m to 4km in the coastal seas of Singapore. The channel probe signals are mainly binary phase shift keying (BPSK) modulated m-sequences. They provide a large bandwidth-duration signal that is ideal for delay-Doppler measurements, giving adequate delay and Doppler resolution. Our channel measurements and analysis have shown that delay and Doppler spread decreases as the distance increases. This implies that at longer distances (up to 4km), the channel is able to support higher bit rates. . In contrary, COTS modems generally degrade to lower bit rates when the transmission range increases in our local shallow water environment.

I. INTRODUCTION

Very-shallow water acoustic communication channels (where the water depth is less than 30m and the range-depth ratio exceeds 10:1) are known to exhibit fading due to time-varying multipath arrivals [1]. The shallow water acoustic channel is generally characterized as a multipath channel due to the acoustic signal reflections from the surface and the bottom of the sea. Because of wave motion, the signal multipath components undergo time-varying propagation delays, resulting in signal fading.

In this paper, we present sea channel soundings and measurements for obtaining the fading characteristics of the shallow underwater channel. In addition, we measured the ambient noise characteristics at different locations. In Section II, we will briefly describe the experimental setup for the sea trials. In Sections III and IV the channel analysis for delay and Doppler spreads will be presented. In Section V, the signal envelope fading is statistically compared to Ricean and Rayleigh fading. In Section VI, the ambient noise data is analyzed. This is followed by a conclusion to summarize the paper.

II. EXPERIMENTAL DESCRIPTION

The experiments were conducted in the coastal sea of Singapore. The transmitter resides on one ship and the receiver on the other (see Figure 1). An omni-directional medium frequency 18.5kHz projector was used to transmit the signal (with a source level of up to 180dB re $1 \mu Pa$ 1m). The receiver is a three band nested linear vertical array of nine hydrophones. In this experiment, we only utilize the 18.5kHz receiving band. For both dry ends equipment, we have a lunch box PC with a National Instrument multi-function data acquisition PCI card. In the sea trial, the receiving ship, ship B, remains at a fixed position while the transmitting ship, Ship A, will move to different locations. The multi-channel received signal is low pass filtered at 50kHz and then acquired at a sampling rate of 200kHz by the receiver PC.

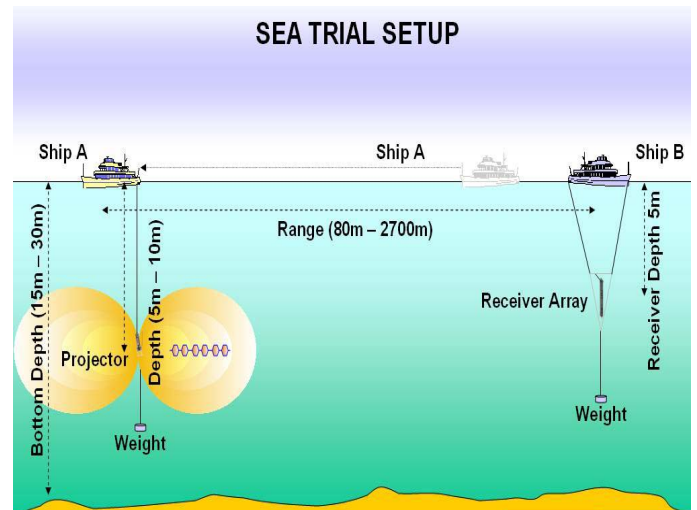


Fig. 1. Experimental set up for channel characterization.

III. MULTIPATH POWER DELAY PROFILES

Multipath power delay profiles (MPDP) of the channels were obtained by making use of broadband BPSK signals modulated with pseudo noise (PN) like m-sequences [2]. The symbol rate used was 4625 bps. The carrier frequency was 18.5kHz. This type of sequence approximately provides us with 0.43ms of delay resolution. Computation of the MPDP was based on [3] whereas time dispersion parameters were detailed from [4]. The m-sequence length was 255 (55

milliseconds) and was generated using the primitive polynomial of degree 8, or [435] in octal representation.

Based on ray paths modeling described in [5], we deduced that PN periods of 55ms are adequately long for multipath profiling and processing gain for all cases from 100m to 4km (see Figure 2). The signal is transmitted and acquired for 60 seconds for the various distances.

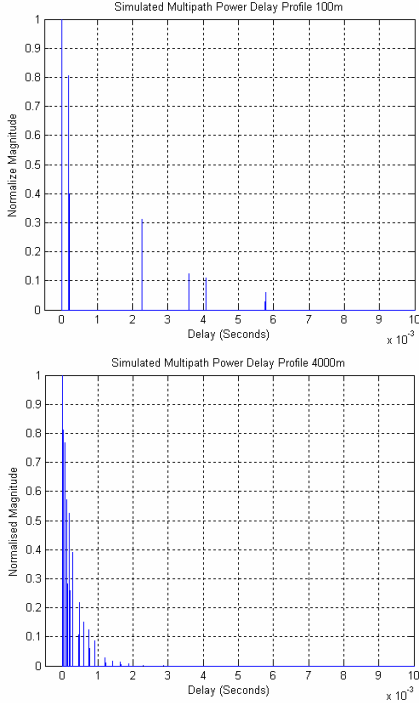


Fig.2. Simulated multipath profiles for 100m and 4000m respectively

The MPDP for each m-sequence frame were computed based on [3]. Each MPDP can be placed next to each other over time to allow the reader to interpret the time history (y-axis) changes in multipath arrivals (in terms of delay (x-axis) and magnitude changes (intensity of z-axis)) (see Figure 3). It can be noted that the MPDP frames are shifted in time due to transmitter and receiver motion, even though the ships are anchored (Figure 3). Hence, an additional step of aligning the frames was needed to align the first arrivals of all MPDP frames. The MPDP frames were re-aligned in a minimum square error (MSE) fashion by comparing the first frame with the subsequent frames (Figure 4).

We refer to Cox [2] who used the following to compute the average power delay profile using a set of envelope delay profiles,

$$P(\tau) = \frac{1}{N} \sum_i E_i^2(\tau) = \left\langle |h(\tau)|^2 \right\rangle_i, \quad (1)$$

where $h(\tau)$ is the bandpass impulse response and $E_i^2(\tau)$ is the i^{th} power delay profile.

The average power delay profile can be viewed Figure 5.

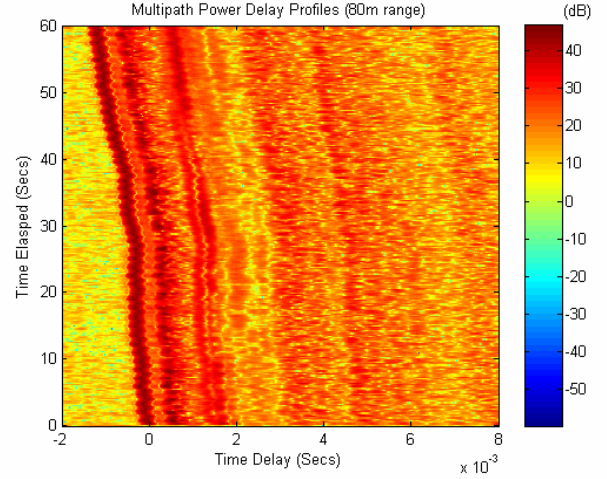


Fig. 3. Multipath delay profiles with time shifts due to ships' motion.

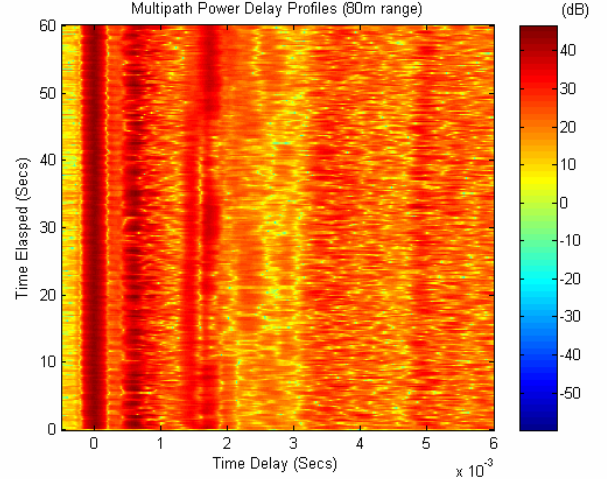


Fig. 4. . Multipath delay profiles after MSE alignment.

A. Delay Spread

Two different ways were used to quantify the delay spread. The first is the excessive delay spread T_m (20dB). It is the time span whereby the multipath energy remains above a certain threshold (in this case we use 20dB) with respect to the strongest arrival. T_m is preferred in designing waveforms that are sensitive to inter symbol interference (ISI).

However, a more reliable measure of delay spread is the root mean square (rms) delay spread, σ_τ instead of T_m [4].

$$\sigma_\tau = \sqrt{\overline{\tau^2} - (\overline{\tau})^2} \quad (2)$$

where

$$\overline{\tau^2} = \frac{\sum_k P(\tau_k) \tau_k^2}{\sum_k P(\tau_k)} \quad (3)$$

and

$$\bar{\tau} = \frac{\sum_k P(\tau_k) \tau_k}{\sum_k P(\tau_k)} \quad (4)$$

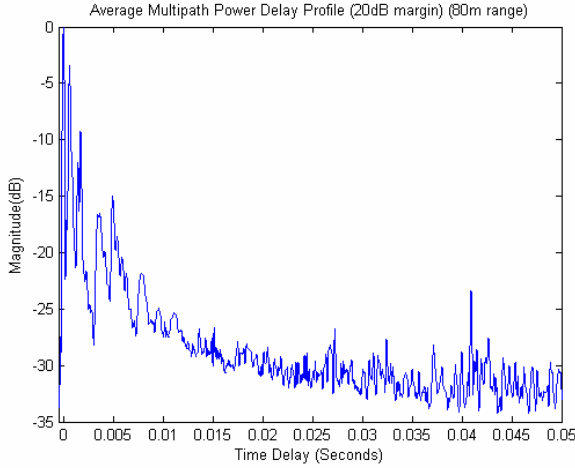


Fig. 5. Average multipath power delay profile

In practice, values for $\bar{\tau}$, $\overline{\tau^2}$, and σ_τ depend on the choice of noise threshold used to derive $P(\tau)$. The noise threshold is needed to prevent the thermal noise from being included as part of the multipath component. If the threshold is set too low, the rms delay estimated may be too high. Time dispersion parameter estimation usually requires a good noise margin. Otherwise, the estimation will be unrealistically high. Here, the threshold margin is set to be 20dB. Figure 6 shows the delay profiles for 80m and 4000m after flooring out the noise. The reduction of the delay spread at 4000m is expected as the range-depth ratio is larger, thereby reducing the time difference of arrivals between the direct and reflected rays.

B. Coherence Bandwidth

The coherence bandwidth is a statistical measure of the range of frequencies over which the channel can be considered “flat” [6]. The coherence bandwidth is taken to be the reciprocal of five times the rms delay spread, σ_τ .

$$B_c = \frac{1}{5\sigma_\tau} \quad (5)$$

Note that the coherence bandwidth estimates here are “ball park estimates”. Spectral analysis and simulation would be required to determine the actual impact the time varying multipath has on a particular transmitted signal.

C. Overall Delay Spread Results

The time averaged MPDPs were used to compute the rms delay spread, which in was in turn used to determine the coherence bandwidth using (5). Table 1 summarizes the delay measurements for distances from 80m to 4000m.

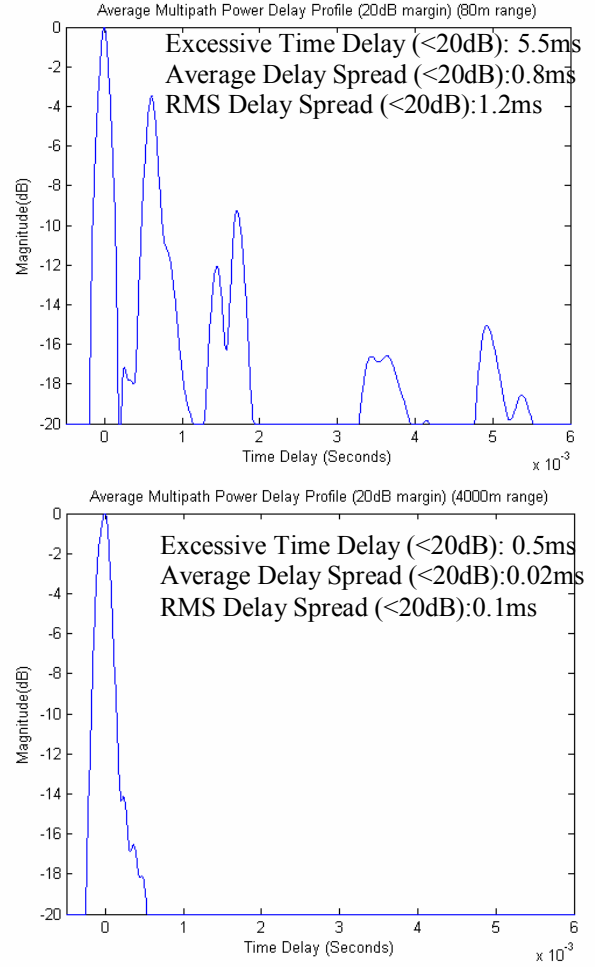


Fig. 6. Average Multipath Power Delay Profiles (Top:80m, Bottom:4000m) after flooring at 20dB.

Table 1. Delay spread and coherence bandwidth results for different ranges

Range (m)	T_m (ms) Excessive Time Delay	σ_τ (ms) RMS Time Delay	Approx Coherence Bandwidth (Hz)
80	5.5	1.2	167
130	7	1.9	105
600	3	0.85	235
1030	3.5	0.85	235
1510	2.5	0.38	526
1740	1.3	0.13	1538
2740	0.5	0.10	2000
4000	0.5	0.10	2000

It can be noted that the delay spread generally decreases as distance increases. Correspondingly, the coherence bandwidth of the channel increases with distance. Due to the 0.43ms delay resolution of the BPSK signal, the actual rms delay spread at 4km may be even smaller than estimated here.

Unfortunately, the projector's limited bandwidth does not permit a higher delay resolution BPSK signal to be used.

Depending on the symbol rate, $T_m > T_s$ will lead to frequency selective fading while $T_m < T_s$ will effect frequency non-selective fading or flat fading. Other than indicating the type of fading, T_m determines the guard time in waveform design and if required, the length of a receiver's equalizer. Frequency domain nulls are prevalent in a multipath environment and it is more severe when the multipath arrivals are stronger (deeper nulling) and sparsely located in delay time (frequent nulling). Therefore, with shorter delay spread in time, the frequency nulls will be further apart creating a larger coherence bandwidth. The coherence bandwidth is useful when designing a modulation scheme which utilizes frequency diversity. For example, in orthogonal frequency division multiplexing (OFDM), a high data rate signal is broken into many narrowband low rate signals to counter ISI. For a narrow band signal, distortion is usually minimized if the bandwidth of the signal is less than the coherence bandwidth.

IV. DOPPLER EFFECTS

The Doppler effects of the channel were captured by transmitting, acquiring and analyzing m-sequence BPSK signals. These large bandwidth-duration BPSK signals are able to provide high Doppler and delay resolution [7]. It is similar to the BPSK signals used to measure the multipath power delay profiles, but the sequence length is much longer. The m-sequence length is 16383 and is generated using primitive polynomial of degree 14, or [42103] in octal representation [2]. This type of long sequence can approximately give 0.43ms of delay resolution as well as 0.3Hz of Doppler resolution. The method for delay-Doppler computation is detailed in [7].

A. Doppler Spread

The mean frequency shift of a received signal due to relative motion between the receiver and the transmitter over some window of time is referred to as the Doppler shift, whereas the fluctuations of frequency around this Doppler shift is referred to as the Doppler spread. Doppler spread arises from variations in the height of the surface reflection point, which is caused by wind driven waves. In our case, it can also be caused by the rocking motion of the projector and hydrophones being tethered from ships. These will, in turn, cause time-variations in the direct and reflected path lengths. As a result, the signal will be phase modulated and the bandwidth of this phase modulation (via Carson's rule) will be known as the estimated Doppler spread, f_d [8]. Doppler shifts and spread indicates the time variations in the multipath structure. These Doppler effects increases with the centre frequency.

The Doppler spectrum (see Figure 7) will provide some form of reference for the communication designer in implementing Doppler correction algorithms. Doppler spread, f_d , is defined here as the null to null bandwidth.

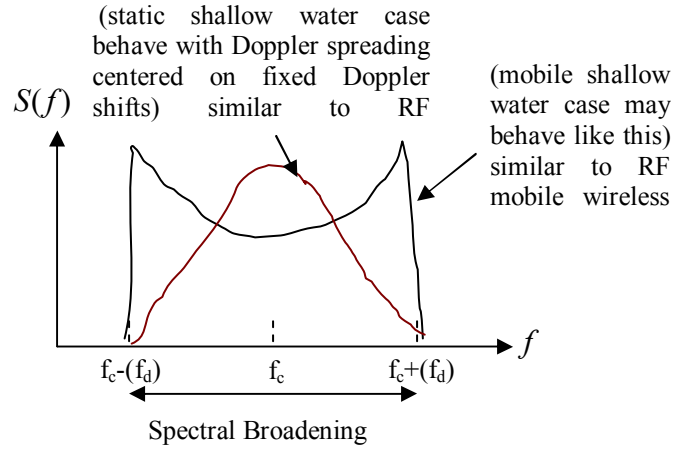


Fig. 7. Typical Doppler Spectrum

B. Coherence Time

Coherence time is the expected time duration within which two signal remains correlated. Coherence time can be approximated from Doppler spread using (6). A shorter coherence time will translate to a multipath structure that varies more frequently.

$$T_0 \approx \frac{0.5}{f_d} \quad (6)$$

If $B = 1/T_{\text{symbol}} < f_d$, then the channel develops fast fading which could lead to severe distortion, irreducible BER and synchronization problems.

If $B > f_d$, then slow fading (the time duration that the channel remains correlated is long compared to the transmitted symbol) occurs and the primary degradation is low SNR. No signal distortion is present.

The delay-Doppler plots at 90m and 2740m are illustrated in Figures 8 to 11. These gave an overview of Doppler spreading trends versus distance. The Doppler results for all the distances are tabulated in Table 2. It can be noted that the Doppler spread will reduce with increasing distance and the Doppler effects on individual paths were different. The Doppler shift depends on the relative velocity between the transmitting and receiving platform. In most cases, our anchored positions are stationary except for minor drifts due to tidal currents. Do note that Ship B was not anchored in the 4000m case as it was situated in the main fairway for ships. As such, it was drifting fast, causing the Doppler spread to increase.

In general the maximum Doppler spread (null to null) is about 9Hz for the shortest range experiment (80m) and goes down to about 2-3 Hz for the longest range experiment (2740m). The Doppler shift is about +/-2Hz for all the ranges. In a single carrier communication system where the bandwidth is high, the Doppler effects are very small and slow fading can be assumed. However in multi-carrier communication, if the

sub-carrier bandwidth is small enough, fast fading may occur. Doppler effects are expected to increase in the mobile case and will be a function of relative velocity.

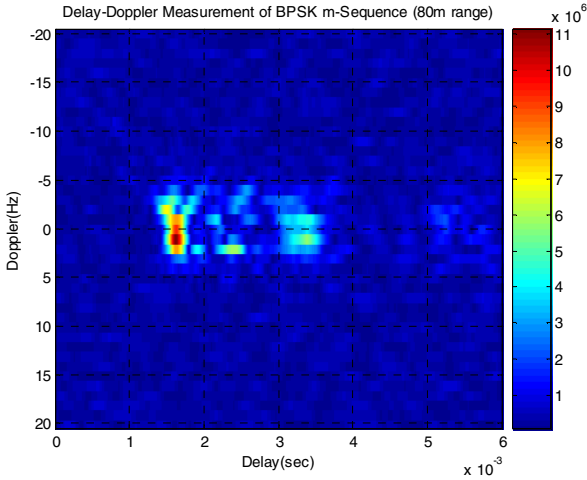


Fig. 8. Delay Doppler Measurement (80m Range)

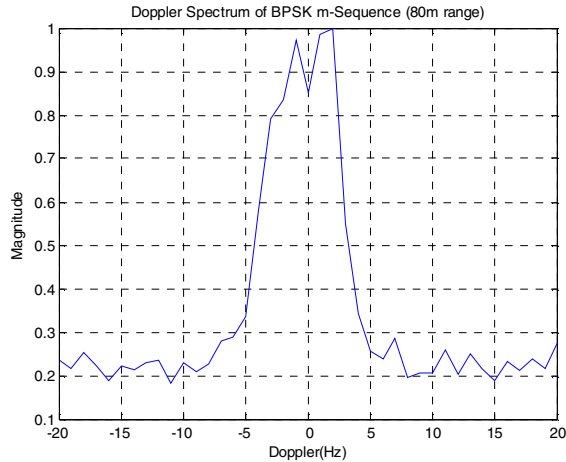


Fig. 9. Doppler spectrum estimate (80m Range)

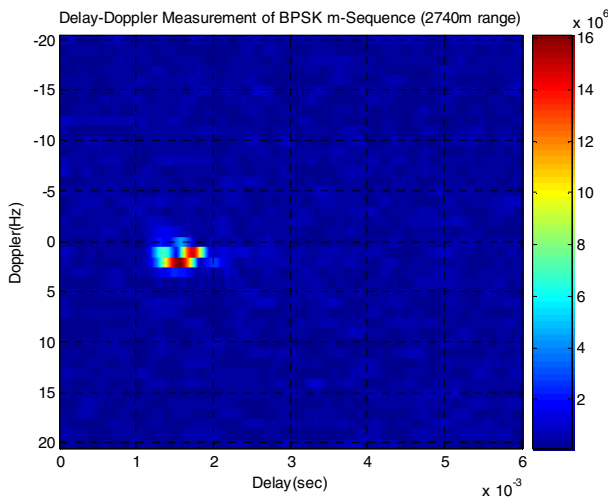


Fig. 10. Delay Doppler Measurement (2740m Range)

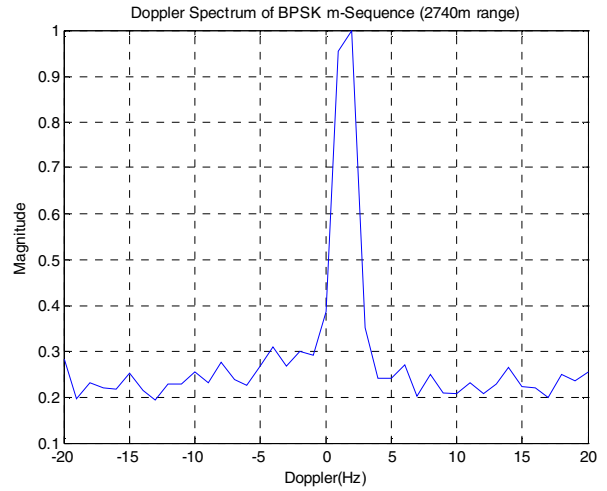


Fig. 11. Doppler spectrum estimate (2740m Range)

Table 2. Doppler and coherence time results for different ranges

Range (m)	Doppler Spread $2f_d$ (Hz)	Doppler Shift (Hz)	Coherence Time (sec)
80	9	-1,+2	1/9
130	8	-1	1/8
600	4	-2	1/4
1030	3	0	1/3
1510	2	-1	1/2
1740	2	+1	1/2
2740	3	+2	1/3
4000*	4	0,+3	1/2

*Ship B is not anchored and drifting fast.

Our channel measurements and analysis results in Table 1 and Table 2 have shown that delay and Doppler spreads decreases at longer distances. This means that at longer distances (up to 4km), the channel is capable of supporting higher bit rates. At shorter distances, techniques to mitigate ISI and Doppler may be needed in order to achieve the same level of performance as at longer distances.

V. SIGNAL ENVELOPE FADING

Using the same set of data from Section III, we begin by passing the data through a band pass filter to remove all out of band noise and interference.

The base band signal is then extracted from the received signal by multiplication with the carrier, followed by low pass filtering (10 kHz). The best sampling instance is obtained by correlating the received signal with the length-255 m-sequence and searching for the correlation peaks. The best sampling instance is updated for every frame received.

The samples around this best sampling instance are collected and the magnitude is calculated to determine the envelope of the received signal. The envelope is scaled such that it is normalized about the median.

A. Rayleigh and Rician Fading

Two common stochastic channel models used to characterize a multipath fading environment are the Rician and Rayleigh models [4]. The Rician model is typically used when there is a strong line of sight (LOS) component present while the Rayleigh model assumes no such component exists.

Rician random variables can be generated using two Gaussian random variables with non-zero means and common variance. The Rice distribution can thus be described using the non-centrality parameter, s , which is a function of the two means, and the common variance. Another parameter, the Rician factor, K , is also commonly used to describe the distribution and can be determined by knowing s and the variance.

Rayleigh random variables, on the other hand, can be generated using 2 Gaussian random variables with zero means and common variance. Varying the variance is sufficient to generate different Rayleigh pdf plots.

The best fitting Rician and Rayleigh pdfs are then determined by varying the various parameters in steps of 0.01 and calculating the corresponding mean square error (MSE). The parameters yielding the lowest MSE correspond to the best fit probability density functions (PDFs). These PDFs and cumulative distribution functions (CDFs) are plotted out and presented in Figure 12 to Figure 15 together with their corresponding parameters and MSEs.

The results are summarized in Table 3. From the table, the results indicate fading to be Rayleigh or weakly Rician at shorter distances with the exception of the 600m data set, and Rician fading at the longer ranges with the exception of the 4000m data set.

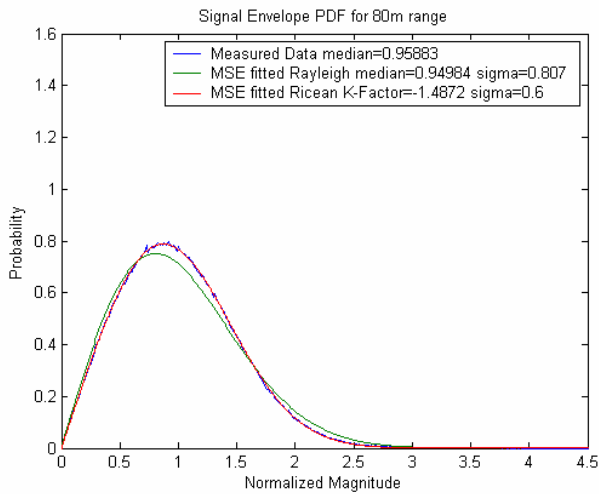


Fig 12. Comparative and measured PDFs for signal envelope received at 80m.

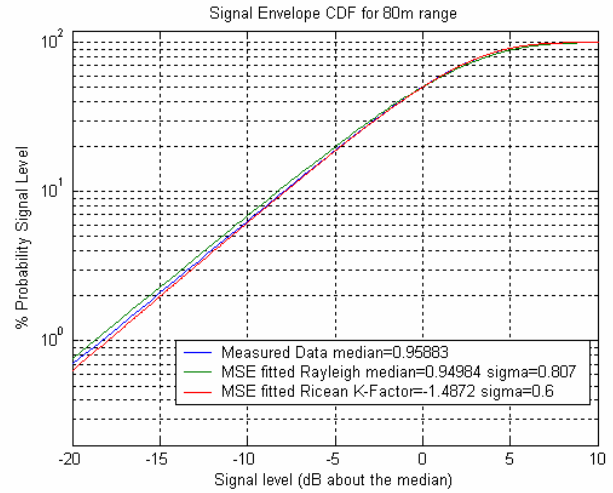


Fig 13. Comparative and measured CDFs for signal envelope received at 80m.

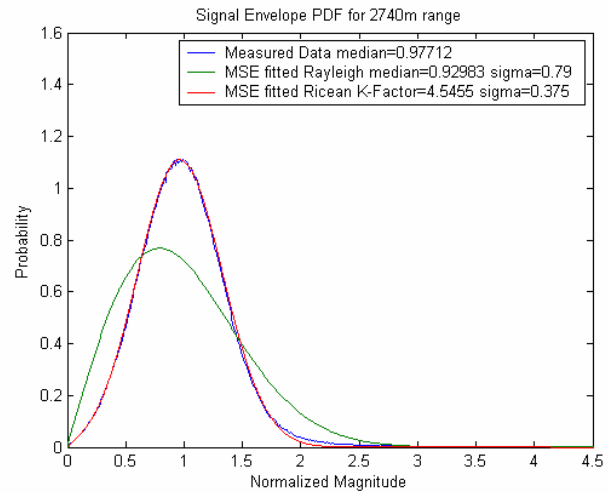


Fig 14. Comparative and measured PDFs for signal envelope received at 2740m

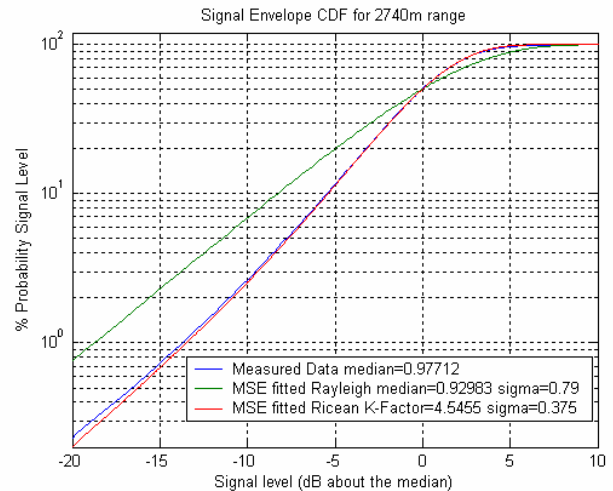


Fig 15 Comparative and measured PDFs for signal envelope received at 2740m

Table 3. Overall results for signal envelope fading for different ranges

Range (m)	MSE Fitted Rayleigh Sigma	MSE Fitted Ricean K-Factor(dB)	MSE Fitted Ricean Sigma	Approx Fit
80	0.807	-1.487	0.600	Rayleigh
130	0.803	-4.167	0.674	Rayleigh
600	0.815	2.757	0.453	Ricean
1030	0.802	-6.787	0.726	Rayleigh
1510	0.807	2.192	0.467	Ricean
1740	0.802	6.253	0.327	Ricean
2740	0.790	4.545	0.375	Ricean
4000*	0.885	-32.571	0.751	Rayleigh

*Ship B is not anchored and drifting fast

VI. AMBIENT NOISE

In [9], it was noted that low frequency ambient noise in shallow Singapore waters were dominated by shipping and reclamation noise, while at higher frequencies; the predominant noise is snapping shrimp noise. A characteristic of snapping shrimp noise is that it is highly impulsive, resulting in a heavy tailed distribution. This implied that the Gaussian distribution, which is commonly used to characterize noise in most environments, is a poor fit for the ambient noise in Singapore waters. This was backed up by data collected in [10], which also proposed the use of alpha-stable distribution to characterize the impulsiveness of snapping shrimp noise.

We conducted ambient noise measurements in Singapore waters over various locations. The pdf graphs of the measured ambient noise were then plotted. By comparing them with simulated pdf plots of Gaussian and alpha-stable distributions, the best fitting distribution could be determined.

Stable distributions are a class of probability distributions that generalize the normal distribution. Alpha-stable distributions are described by four parameters. As our noise distribution is zero-mean and symmetric, two of the parameters can be set to be zero. Thus, only two parameters need to be estimated: the characteristic exponent (alpha) and the scale parameter, c , from our measurements to yield the best fit stable distribution. These were obtained using the method described in [11]. To generate random stable variables, the methods described in [12] and [13] were used. Both the scale parameter and characteristic exponent are positive numbers, with alpha having an additional restriction: the maximum value it can take is 2. When alpha is 2, the stable distribution reduces to the familiar Gaussian distribution.

Gaussian random variables were generated using two methods: 1. by calculating the variance of the measured noise and generating Gaussian variables with similar variance, and 2. generating stable random variables as described previously, but equating alpha to 2 instead of estimating it using [11].

Our findings are illustrated in the figure shown below. It shows the PDF of the measured noise, the estimated stable PDF and the estimated Gaussian PDFs. (See Fig. 16)

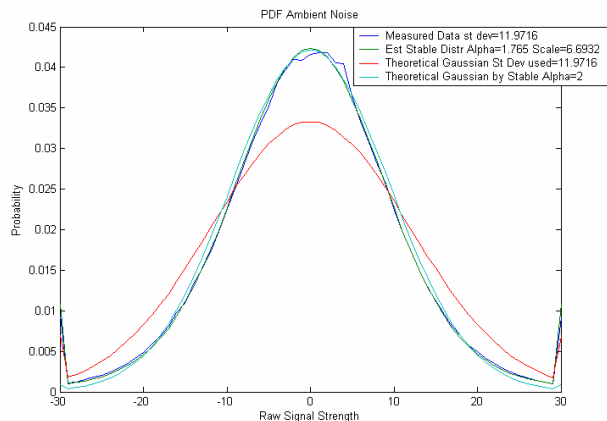


Fig. 16. Comparison of various histograms versus measured ambient noise histogram.

The best fit alpha stable pdf had an alpha of between 1.6 and 1.8 and yields a much better fit than the Gaussian pdfs. Gaussian pdfs tend to be poor fits. As the pdfs were drawn from histogram plots, the tail ends appear as spikes in the diagrams. These could be ignored as they simply indicate the heaviness of the tails and are not found in the actual pdfs. If the pdf of the model exhibits similar spikes as the noise pdf, it indicates good fit in the tail regions.

VII. CONCLUSION

Based on our static medium frequency (9-28kHz) channel measurements in very shallow waters (15-30m) for distances from 80m to 4km in the coastal sea of Singapore, we have presented delay, Doppler, fading and ambient noise analysis that described the impulse response and temporal behavior of the channel. We have observed that the delay and Doppler effects are less at longer distances. It was also noted that the LOS component is more likely to be observed at the longer distances. Ambient noise is non-Gaussian with a heavy tailed distribution and a highly impulsive behavior. Communication system designers should take note of the channel characteristics at longer distances (>1500m up to 4000m) to transmit at higher data rates. On the other hand, it would be a serious challenge to design a modem for shorter distances that can achieve the same level of performance that was possible at longer distances.

ACKNOWLEDGMENTS

We would like to express our gratitude to Mr Koh Tiong Aik and Mr Zhong Kun for their help with the sea trial experiments and data transmissions/acquisitions. In addition, we would like to thank Dr Ng Boon Chong and Mr Chia Chin Swee for their invaluable advice during the entire course of this work. This work is fully sponsored by DSO National Laboratories.

REFERENCES

- [1] Josko A. Catipovic, "Performance Limitations in Underwater Acoustic Telemetry", *Oceanic Engineering, IEEE Journal of*, Vol:15, No.3, pp.205-216, July 1990.
- [2] Roger L. Peterson, Rodger E. Ziemer, David E. Borth, *Introduction to Spread Spectrum Communications*, 1st ed., New Jersey: Prentice Hall, 1995, pp.113-121.
- [3] Donald C. Cox, "Delay Doppler Characteristics of Multipath Propagation at 910MHz in a Suburban Mobile Radio Environment", *IEEE Trans. on Antennas and Propagation*, vol. 20, Issue 5, pp.625-635, September 1972.
- [4] Theodore S. Rappaport, *Wireless Communications*, 2nd ed., New Jersey: Prentice Hall, 2002.
- [5] A. Zielinski, Y. H. Yoon and L. Wu, "Performance Analysis of Digital Acoustic Communication in a Shallow Water Channel", *Oceanic Engineering, IEEE Journal of*, Vol:20, No.4, pp.293-299, October 1995.
- [6] Michel C. Jeruchim, Philip Balaban, K. Sam Shanmugan, *Simulation of Communication Systems*, 2nd ed., New York: Kluwer/Plenum, 2000.
- [7] G. Jourdain, J.P. Henrioux, "Use of Large Bandwidth-Duration Binary Phase Shift Keying signals in Target Delay-Doppler Measurements", *J. Acoust. Soc. Am.* 90(1), 1991.
- [8] Milica Stojanovic, "Recent Advances in High Rate Underwater Acoustic Communications", *Oceanic Engineering, IEEE Journal of*, Vol:21, Issue 2, pp.125-136, April 1996.
- [9] Tan Soo Peng, Koay Teong Beng, P. Venugopalan, Mandar A. Chitre and John R. Potter, "Development of a shallow water ambient noise database", *Underwater Technology 2004, International Symposium on*, pp.169-173, Taiwan, April 2004.
- [10] Mandar Chitre, John Potter, Ong Sim Heng, "Underwater acoustic channel characterization for medium-range shallow water communications", *MTS/IEEE TECHNO-OCEANS '04*, Vol:1, pp40-45, November 2004.
- [11] Fama E. F. and R. Roll, "Parameter estimates for symmetric stable distributions," *J. Am. Stat. Assoc.* 66, pp. 331-338, 1971.
- [12] Graham Cormode, "Generating Stable Distributions", 2005. <http://dimacs.rutgers.edu/~graham/code.html>.
- [13] John P. Nolan, "Stable Distributions Models for Heavy Tailed Data", Chapter 1, Jan 11, 2005, book in progress, Unpublished.